minerals

MDPI

Article

Viability of Morisca Powder Tailings for Ceramic Applications

Antônio Alves de Carvalho Jr. [1,2], Kelson de Sousa Leite [1,2] and José Milton Elias de Matos [2,3,*]

[1] IFPI Ceramic Materials Laboratory, Federal Institute of Education, Science and Technology of Piauí—IFPI, Av. Pedro Freitas, Teresina 64019-368, Brazil
[2] Technology Center—UFPI, Materials Science and Engineering, Federal University of Piauí—UFPI, Teresina 64064-260, Brazil
[3] Chemistry Department, Federal University of Piaui—UFPI, Teresina 64049-550, Brazil
* Correspondence: jmematos@ufpi.edu.br

Abstract: In Juazeiro de Piauí and Castelo do Piauí, two cities in northeast Brazil, mined morisca rock is widely used in civil construction for external coating applications. Aiming at a sustainable practice for its extraction, which includes the economical use of the tailings from its mining, this work presents a solution for the use of discarded materials from processing morisca from Piauí. In this context, an analysis of the results of using morisca as a substitute for clay materials for applications in red ceramics are presented. For the analyses, XRF, XRD, microgranulometry, limits of consistency, TG, DTG, and a set of technological tests inherent to ceramic materials were used. It was concluded that morisca powder is viable as a clay substitute for red ceramic applications.

Keywords: red pottery; sintering; morisca; mourisca; quartzite; morisca powder

check for updates

Citation: Carvalho Jr., A.A.d.; Leite, K.d.S.; Elias de Matos, J.M. Viability of Morisca Powder Tailings for Ceramic Applications. *Minerals* **2023**, *13*, 459. https://doi.org/10.3390/min13040459

Academic Editors: Daniela Guglietta, Stefano Milia, Giovanna Cappai and Adalgisa Scotti

Received: 27 January 2023
Revised: 1 March 2023
Accepted: 8 March 2023
Published: 24 March 2023

Copyright: © 2023 by the authors. Licensee MDPI, Basel, Switzerland. This article is an open access article distributed under the terms and conditions of the Creative Commons Attribution (CC BY) license (https://creativecommons.org/licenses/by/4.0/).

1. Introduction

The Brazilian lithological industry is still promising, because even with the economic crisis, in terms of ornamental and coating stones, Brazil exported a total of USD 1,014,293 and 2,165,405 t in 2019, with a positive variation in billing but a contraction in physical volume, when compared with 2018 [1].

In the state of Piauí, in Brazil, specifically in the regions that include the cities of Castelo do Piauí and Juazeiro do Piauí which are located in the centre of the northern area of the state, the extraction and processing of rock called arcosian sandstone (extracted quartzite)—commercially known as morisca stone—takes place [2]. It reached a production of 100,000 t in 2019, along with the slate produced in the state [1].

Arcosian sandstones are detrital sedimentary rock formations composed of solid particles such as sand and gravel, originating from parent material by mechanical and chemical weathering, composed mainly of quartz and feldspars [3]. In the region mentioned above, this ornamental stone has classic chromatological characteristics, with macroscopic colour tones from yellowish to slightly reddish, grey with a tendency to black, and multicolour [4]. Mafic minerals cause such colours, but morisca is not classified as mafic, as it has a high silicon content and is a rock that occurs in the most superficial layer of the earth (extrusive). For simplification of nomenclature, from now on we will call it morisca.

In general, its extraction still occurs without the implementation of technological resources, carried out in the open (Figure 1A) after cleaning the area chosen for mining, followed by squaring the structural plans of morisca through manual and rudimentary actions, with the use of suitable metal tools to obtain it. At this stage, it is already possible to detect many tailings (Figure 1B) accumulated near the quarry areas [5]. With the blades removed, these are taken for processing; they can be ground and polished, although they can be found commercially without any processing. More waste is generated during the grinding and polishing process, namely, morisca powder (Figure 1C), along with a large volume of used water. Around 20,000 litres of water is used per day, if all the machines are

on, coming out of two storage tanks (75,000 litres and 150,000 litres) filled with decantation water, as all the water is reused in morisca processing procedures.

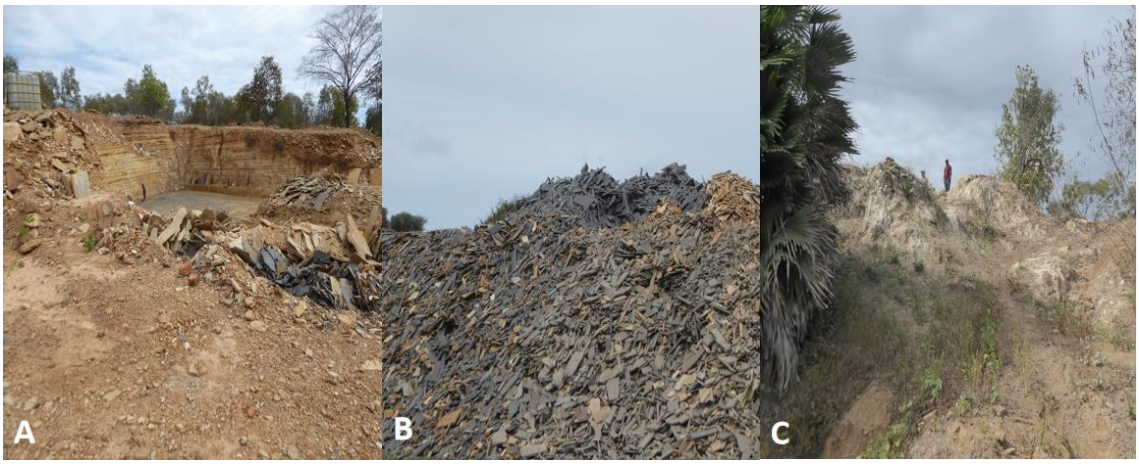


Figure 1. Panoramic view displaying the quarry of stratified quartzite (**A**), tailings (**B**), and tailings in powder form (≅29% quartz (Figure S1)) (**C**), resulting from the mining process. Altos, State of Piauí, Brazil.

From this perspective, the environmental liabilities of this mineral prospect have grown each year, requiring the development of technological strategies for the reuse of the generated tailings, those strategies preferably being economically viable since only then can investment be undertaken to remediate this environmental problem.

In this scenario, as the traditional ceramic industry based on clay–silica–feldspar consumes a large amount of natural raw materials, its raw materials consisting of a diversified composition, tolerating fluctuations in its composites and the addition of different types of waste, morisca presents itself as a candidate to provide a solid waste reuse stream [6].

To exemplify that the statement above has been consolidated, we identified several types of mining tailings tested for construction materials in the literature: incorporation of quartzite fines for the production of ceramic materials [7,8]; copper–nickel slag aggregation in a multi-component formulation for the production of building ceramics, with low percentages of nickel (0.14% of NiO) and copper (0.06% of CuO) in the slag [9]; application of copper–nickel ore treatment tailings (0.09% and 0.20%), nepheline apatite and iron quartzite in clay-free construction ceramics, by means of compression molding [10]; association of clayey materials with the primary sludge from the red ceramic paper industry [11]; use of clay from gypsum mining and gypsum residue for the production of red ceramics [12]; addition to the ceramic mass of tailings rich in quartz and heavy metals from mining [13]; use of ash from the solid waste and tailings factories of a Greenland mine to produce clay-based bricks [14]; use of different levels of marble powder to improve the properties of ceramic bricks [15]; use of granite and marble tailings as raw materials to be aggregated with clay in the production of red ceramics [16,17]; and, viability of soapstone and soapstone residues soaked in oil, added to the clay mass for the manufacture of red ceramics [18].

Mining tailings are often incorporated into clayey masses to produce ceramics. Therefore, starting from the premise that the ceramic industry is a receptive sector to the incorporation of residues for the production of its products [19], as well as morisca powder manifesting an inherent characteristic of clayey materials, this objective work studies the technical feasibility of using this material in the red ceramics industry, following Brazilian technical norms, aiming to replace the raw material of this economic segment (clay) with morisca powder derived from processing waste.

2. Materials and Methods

2.1. Feedstock

The morisca powder used was purchased from ECB Rochas Ornamentais do Brasil Ltd., derived between the municipalities of Castelo do Piauí and Juazeiro do Piauí (Brazil) (5°12′37.2″; S 41°42′;12.5″ W), and was the result of the extraction, thinning, and polishing of the rock sheets in the beneficiation process. The sample was submitted to NBR 6457 [20], with the sample dried until achieving hygroscopic humidity and breaking up of the clods. The material was deagglomerated in a ball mill and dried in a laboratory oven at 110 °C ± 10 °C.

2.2. Chemical, Mineralogical, and Thermal Analysis Tests

Samples were passed through a #200 sieve (75 μm) for chemical, mineralogical and thermal tests. The semi-quantitative chemical analysis of the material was performed by the fluorescence technique of X-rays (FRX), using Shimadzu EDX-720 equipment, with a detection limit from Na (11) to U (92) (>0.1%).

The mineralogy was studied by X-ray diffraction (XRD) using a Shimadzu diffractometer, XRD 6000 model with CuKα (λ = 0.15406 nm), collecting diffraction data in 2θ from 5° to 75°, and a power of 1.5 kW with a step size of 2° min^{-1}. To better investigate the morisca peak attributions, another mineralogy study was repeated by X-ray diffraction (XRD) using a step size of 0.02° min^{-1} with the same other parameters. The identification of the crystalline phases was carried out through a search in the database with the X'Pert system, HighScore Plus.

Thermogravimetric analysis (TGA) was performed on a TA Instrument SDT Q600 in a nitrogen atmosphere, with a heating rate of 10 °C/min between room temperature (25 °C) and 1200 °C. The amount of sample used was approximately 10.73 mg in a platinum crucible. For the thermodifferential analysis (DTA), the Calorimeter RB 3000–20 was used, with a heating rate of 10 °C/min from room temperature to 1150 °C.

2.3. Particle Analysis

After the milling process, the material was passed through a #40 sieve and then subjected to a particle size test, performed with a SediGraph III Plus V1.00 using the methodology of sedimentation by gravity monitored by X-rays, and the calculations were conducted based on Stokes' and Beer's laws. It was also possible to determine the material's actual density of 2.65 g/cm^3.

2.4. Consistency Limits

A portion of the material was passed through a #80 sieve, and distilled water was added and mixed to the presumed moisture point of the liquid limit to determine the Atterberg limits. Then, the prepared material was placed in a plastic bag so as not to lose moisture, and left to rest for 24 h, after which it was thrown into the liquid limit apparatus to determine the points of the humidity/number of blows ratio; as the temperature was increased, the humidity determined the liquidity limit at 25 strokes [21]. Portions consisting of 60 g of this material were used to determine the moisture content (h), and 10 g portions were used to determine the plasticity limit. Therefore, it was possible to calculate the plasticity index by the liquidity limit difference minus the plasticity limit [22].

2.5. Specimens and Technological Tests

With the material atomised and passed through a #80 sieve, the individual mass was determined for the dry and wet specimens, which were shaped by uniaxial pressing with an approximate load of 55.1 MPa, in a laboratory hydraulic press, through a prismatic matrix box sized 8 cm × 1 cm (Figure 2A), with an average height after pressing of 1 cm (Figure 2B). Dimensional measurements were carried out with a 0.05 mm resolution caliper. The specimens were weighed with a 0.01 g digital scale and then placed in an oven for 24 h

after drying in the shade, to carry out the dimensional measurements and weighing of the specimens again after drying.



Figure 2. Matrix box for making prismatic specimens (**A**), and examples of burned specimens(**B**).

The firings were carried out at 800 °C, 900 °C, 1000 °C, 1100 °C, and 1150 °C in a muffle furnace, with a heating rate of 4 °C/min. New dimensional measurements and weight measurements were performed. After all these steps, it was possible to calculate the water absorption by Equation (1), the porosity by Equation (2), and the apparent specific mass by Equation (3). The linear drying shrinkage and the linear burning shrinkage were calculated by Equation (4). In contrast, the total shrinkage was derived by Equation (5). The equations cited are found in Table 1.

Table 1. Equations of technological tests.

Variables	Equations		Description
Water Absorption (WA)	$WA = \frac{ww-dw}{dw} \times 100$	Equation (1)	dw = dry weight ww = wet weight av = apparent volume L_i = initial length L_f = final length
Apparent Porosity (AP)	$AP = \frac{ww-dw}{av} \times 100$	Equation (2)	
Apparent Specific Mass (ASM)	$ASM = \frac{dw}{av}$	Equation (3)	
Drying and Firing Linear Shrinkage ($S_{D/F}$)	$S_{D/F}(\%) = \frac{L_i-L_f}{L_f} \times 100$	Equation (4)	
Total Retraction	$R(\%) = S_{Drying} + S_{Firing}$	Equation (5)	

As for the flexural strength, the results were obtained by the three-point bending test, with a speed of 0.5 mm/min, using a EMIC deflectometer, DL 20,000 model, and with a load cell of 200 kN. We emphasise that the procedures adopted for the technological tests had the theoretical contributions of NBR 15270-2 [23] and NBR ISO 10545 [24] standards, as well as the literature on ceramic tests [25].

3. Results and Discussion

3.1. Raw Material Characterisation (before Firing)

Table 2 shows the weight percentage results of the semi-quantitative chemical analysis of the morisca sample. XRF identified a high content of 70.55% silicon oxide (SiO_2), 14.24% aluminium oxide (Al_2O_3), 9.10 % iron oxide (Fe_2O_3), 2.49% potassium oxide, and other oxides with percentages below 2%. Given the SiO_2 content, a component that reduced the plasticity of the sample, the Al_2O_3 contributed to the plastic characteristic of morisca and collaborated with water retention [26], favouring the moulding capacity of pieces made with morisca [27], so the sample had an indication of medium plasticity, confirmed with the Atterberg tests shown in Table 3. Fe_2O_3 occurred in a combined form and was responsible

for the reddish tones of the pieces when fired; in addition, it negatively interferes with plasticity and mechanical strength, so its occurrence rate should be less than 10% [28]; thus, the morisca sample met the suggested limit.

Table 2. Result of the semi-quantitative chemical analysis of the morisca sample by XRF.

Oxides	SiO_2	Al_2O_3	Fe_2O_3	K_2O	TiO_2	MgO	CaO	P_2O_5
(%)	70.55	14.24	9.10	2.49	1.70	1.40	0.33	0.33

Table 3. Granulometric composition in the percentage of the morisca sample.

Sample	Fine Quarry Materials (%) v% $\leq$ 2 µm	Silt (%) 2 µm < v% $\leq$ 20 µm	Sand (%) v% > 20 µm	Average Diameter µm
Morisca	60	37.4	2.6	1.34

The mineralogical analysis results are presented in the morisca diffractogram (Figure 3). A comparison of the diffractogram peaks with the diffraction pattern base identified compatibility with the following phases: quartz (SiO_2—PDF-01-086-1630), anorthite ($CaAl_2Si_2O_8$—PDF-01-086-1706), magnesium titanium oxide (Mg_2TiO_4—PDF-001-079-0830), iron titanium oxide ($FeTi_2O_5$—PDF-01-076-2372), potassium aluminum silicate ($CaAl_2Si_2O_3$—PDF-000-014-0081), aluminum silicate ($K_{57}Si_{135}Al_{57}O_{384}$—PDF-01-073-0491), and three suspiciously recognizable diffraction peaks, that we placed as unidentified, which disappeared after the first burn. Apart from quartz and tridymite, which are phases associated with silicon oxide, the other phases composed the fluxes that incorporated the plastic characteristics manifested by the morisca powder [29].

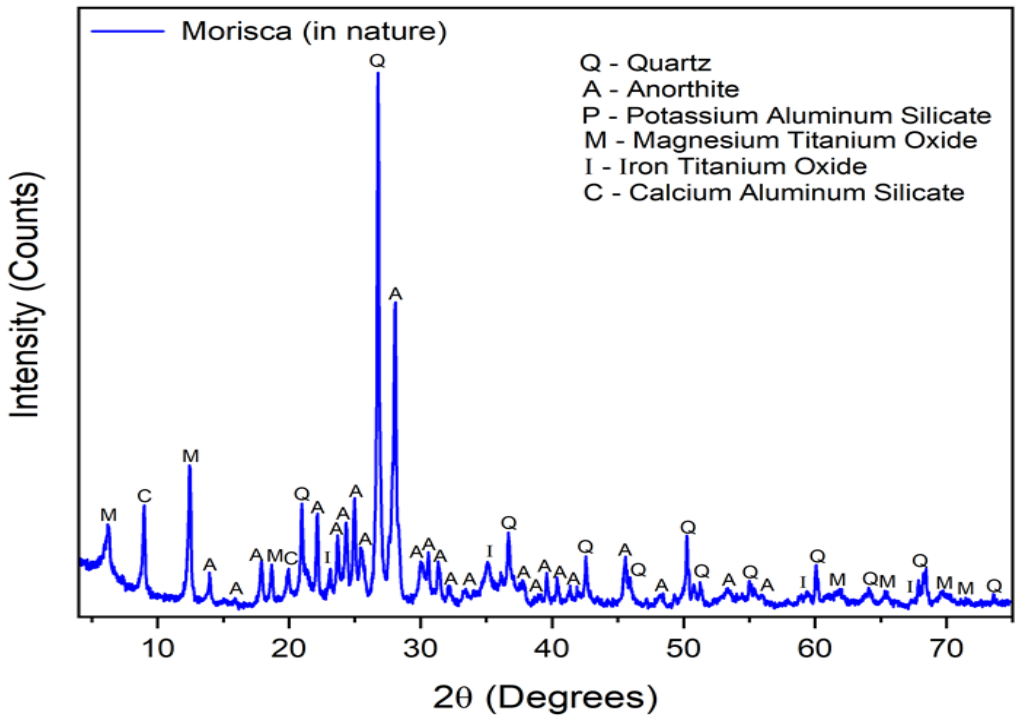


Figure 3. XRD pattern of raw morisca (in nature). Step size of 0.02° min^{-1}.

Despite being a plasticity-reducing agent, we emphasise that quartz is desirable in ceramic materials since it guarantees structural integrity during firing, controlling shrinkage and favouring the pieces' drying. However, it is essential to be careful with the burning rate because at around 573 °C alpha quartz undergoes an exceptionally rapid transformation to beta quartz, causing volume increase and, as a consequence, cracks in the burned parts [30]. Therefore, the diffractogram corroborates the semi-quantitative chemical analysis presented in Table 2.

The micro granulometric characterisation of morisca is presented in Table 3 and Figure 4. We analysed the particle size distribution through the classification proposed by the International Society of Soil Science, which states that granulometric fractions smaller than 2 μm are defined as clay, granulometry between 2 and 20 μm are silt, and granulometric fractions larger than 20 μm are classified as sand [31]. Thus, the sample comprised 60% excellent quarry materials, 37.4% silt, and 2.6% sand, and an average diameter of 1.34 μm. These granulometric characteristics of morisca, mostly smaller than 2 μm, give this material the plastic characteristic of the morisca and water system, making it possible to create products similar to the clays used in the red ceramic industry [32].

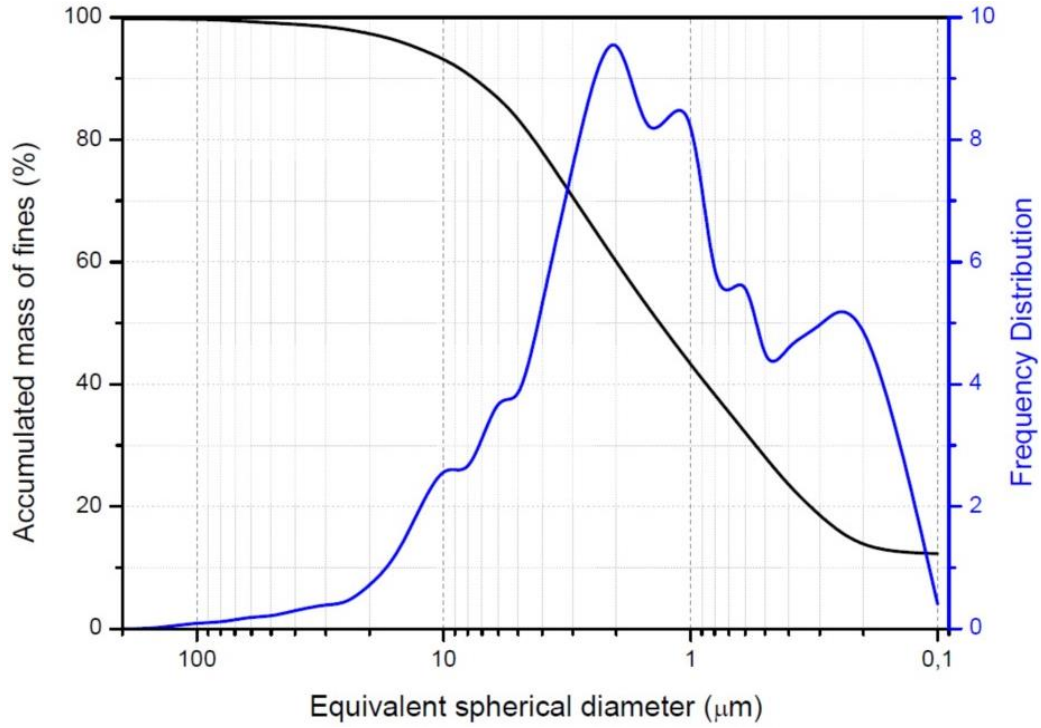


Figure 4. Distribution of morisca particle size.

Based on the results of the Atterberg tests (Table 4), the sample may be classified, in terms of plasticity, as weakly plastic if the plasticity index (PI) is between 1 and 7, moderately plastic if the PI is between 7 and 15, and highly plastic if the PI is greater than 15 [33]. It is worth mentioning that these tests make it possible to identify the plasticity limit (PL) and the liquidity limit (LL), which, together with the PI, indicate the amount of water needed to carry out the moulding of the parts [34]. A value of 24.61% was found for the LP and 38.24% for the LL; these are the minimum and maximum limits in the percentage of water that can be added to the material to keep it in a plastic state. We obtained, for the morisca, a value of 13.63% for the PI, which allowed us to classify the material as moderately plastic. This characteristic can be explained by the high silica content identified in the semi-quantitative chemical analysis (Table 2). However, it was an excellent result because it would be difficult to dry if it had high plasticity, which could produce cracks in the parts.

Table 4. Plasticity index of the morisca sample.

Sample	Liquid Limit (LL) %	Plastic Limit (PL) %	Plasticity Index (PI) %
Morisca	38.24	24.61	13.63

The Atterberg limits tests also facilitate an extrusion prognosis, that is, to identify whether a material is in a more favourable region for the conformation of ceramic pieces by the extrusion method. Although the specimens of this work did not use the extrusion method, which is widely used in the ceramic industry, it was still essential to show that it is possible to use morisca utilising this methodology, as at an industrial level it impacts productivity and workability with the green pieces produced [35]. In this context, Figure 5 presents the result of the morisca extrusion prognosis, which was classified as acceptable for forming parts using the extrusion method even though it was not in an optimal region.

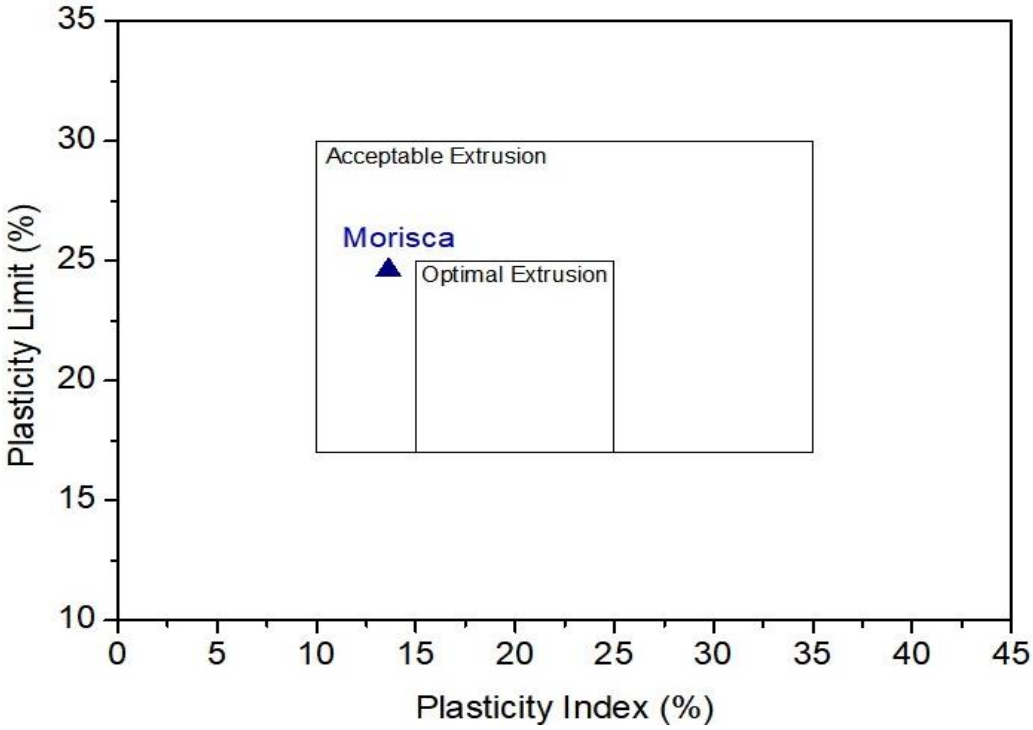


Figure 5. Morisca extrusion prognosis.

The lost mass identified was 0.484 mg (Figure 6), equivalent to 4.51% of the sample mass. It was a slight loss, a desirable characteristic for ceramic applications, and must be related to the elimination of water and evaporation of impurities that may exist in the material.

Figure 7 shows the thermodifferential analysis, where two endothermic peaks were identified. The first peak (482 °C) was associated with the dehydroxylation of clay minerals. The second peak (530 °C) was attributed to the transition from alpha quartz to beta quartz. In this case, it is crucial to maintain a low burn rate in the temperature range that composes the second endothermic peak, avoiding problems that may occur with the quartz transition.

3.2. Characterisation after Burning

Figure 8 compares the morisca diffractograms with morisca after firing at 800 °C, 900 °C, 1000 °C, 1100 °C, and 1150 °C. The crystalline phases identified in the firing at 800 °C were quartz (PDF 01-078-1422), anorthite (PDF 00-041-1486), and potassium aluminium silicate (PDF 00-046-0741); at 900 °C they were quartz (PDF 01-00-033-1161), anorthite (PDF 01-073-00-041-1486), and potassium aluminium silicate (PDF 00-046-0741).

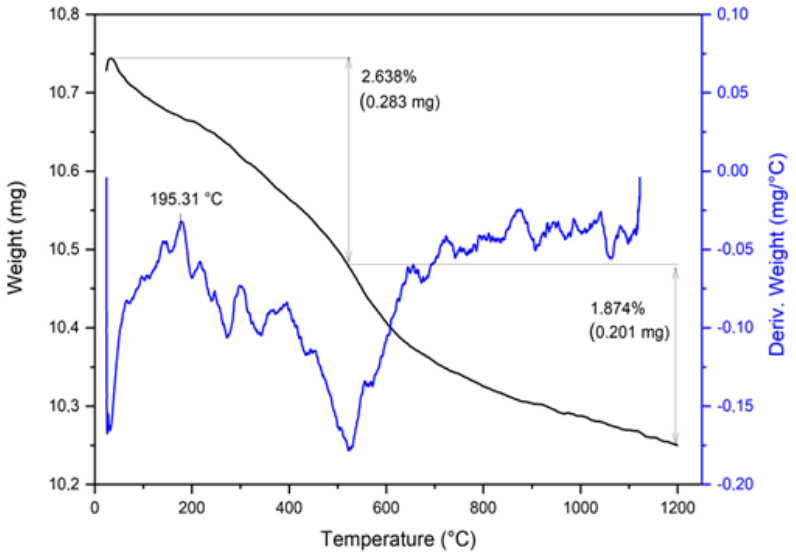


Figure 6. Result of the morisca thermogravimetric analysis.

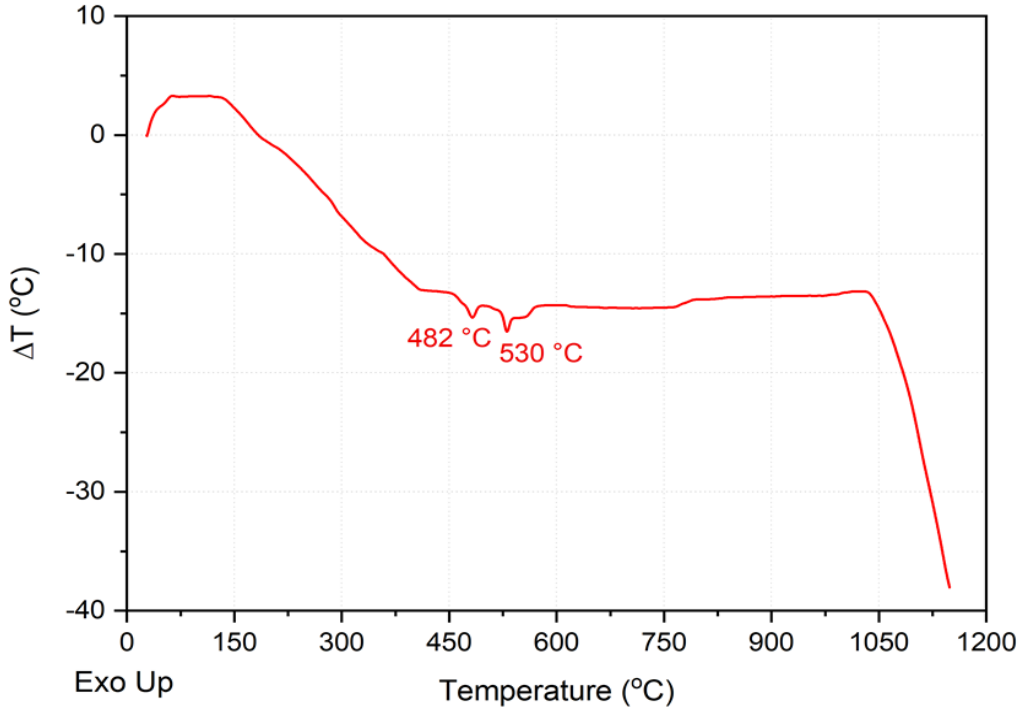


Figure 7. Result of morisca thermodifferential analysis.

Upon firing at 1000 °C, quartz (PDF 01-078-1422), anorthite (PDF 00-041-1486), and potassium aluminium silicate (PDF 01-079-1823) were observed in the same phases. As for the firing at 1100 °C, quartz (PDF 01-083-0539), anorthite (PDF 00-041-1486), and new phases microcline ($KAlSi_3O_8$ PDF 00-022-0675) and hematite (Fe_2O_3 PDF 001-073-0603), were observed.

Quartz peaks existed in all diffractograms, including silicon oxide, an isomorph of quartz, identified in the burning at 800 °C. However, at 1150 °C, only three phases were observed: quartz (PDF 01-079-1910), anorthite (PDF 00-041-1486), and hematite (Fe_2O_3 PDF 01-079-0007). The quartz peaks were smaller, and could be associated with the partial dissolution of quartz to a dense phase, favouring the reduction in porosity in the pieces. The hematite that emerged at this temperature brought the chromatology of the fired pieces to a darker reddish colour.

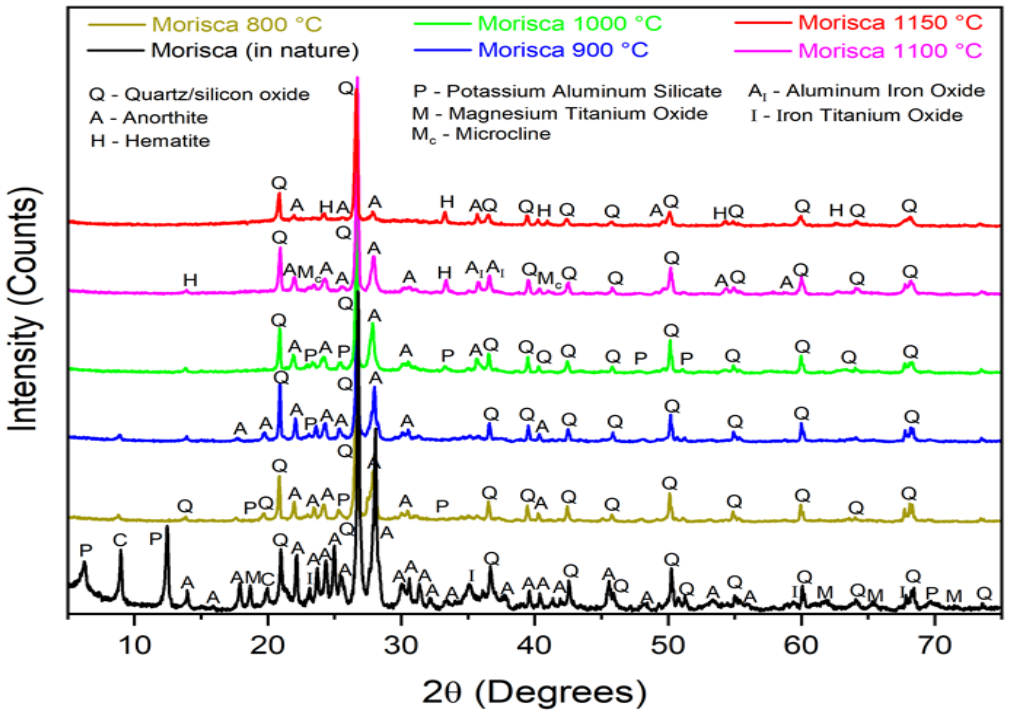


Figure 8. XRD comparison diffractogram of morisca in nature with calcinations at 800 °C, 900 °C, 1000 °C, 1100 °C, and 1150 °C. Step size of 2° min^{-1}.

The results of the apparent porosity (AP), water absorption (WA), and specific mass (SM) tests are shown in Figure 9, which allows us to state that the apparent porosity and water absorption decreased with increasing temperature while the specific mass increased. This behaviour is expected for materials with clayey characteristics after firing.

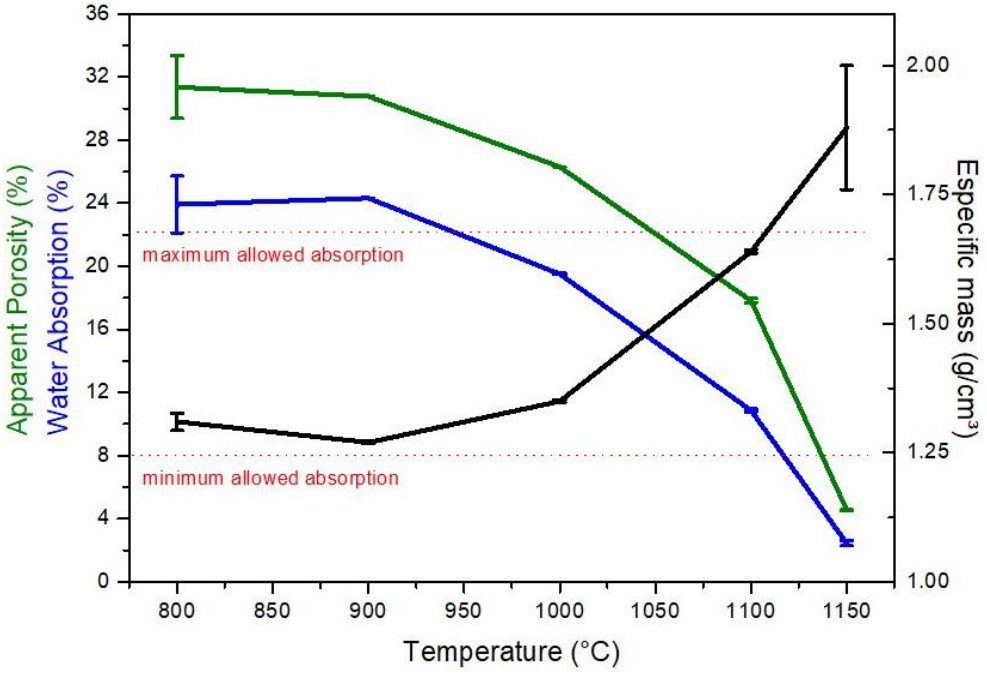


Figure 9. Results of apparent porosity, water absorption, and specific mass tests.

Apparent porosity is closely linked to densification and sintering resulting from the material firing process [36], making it an essential parameter for ceramic applications. In this sense, porosity was reduced from 31.37% at 800 °C, to 4.56% at 1150 °C, which affected

the other mechanical properties of the parts. The behaviour of water absorption, which depends on the porosity of the specimens, maintained the same downward trend in the apparent porosity. Regarding values, the water absorption at 800 °C and 900 °C was above the values allowed in the ABNT standard, which defines that ceramic products, specifically for masonry, must have a water absorption index between 8% and 22% [37]. However, for the production of tiles, the norm only determines the maximum index allowed of 20%, emphasising that these are values for applications in temperate or tropical climates [38]. For masonry, at 1000 °C and 1100 °C, the specimens met the normative specifications, while at 1150 °C, the result was below the lower limit allowed but in regulatory compliance for the production of tiles. The amortisation in the porosity performance directly impacted the specific mass, as the reduction in void spaces in the tested bodies promoted more significant densification of the material, and consequently, an increase in the specific mass due to the decrease in porosity, starting from 1.31 g/cm^3 at 800 °C, to 1.88 g/cm^3 at 1150 °C [39].

The variables AP, WA, and SM (Figure 9) directly impacted the flexural strength of the specimens shown in Figure 10. As for porosity, flexural strength is subject to the normative support of ABNT [32], which advocates a minimum strength of 2 MPa (20 kgf/cm^2) for ceramic products. It can be seen in Figure 10 that the increase in temperature produced an increase in the resistance values of the specimens, but this behaviour did not meet the norm up to 1000 °C. However, at 1100 and 1150 °C, it was possible to identify compliance with the standard. The gain in strength above 1000 °C was strongly linked to the sintering of the clay minerals that emerged—calcium aluminium silicate, microcline, and potassium iron silicate—as predicted in the mineralogical analysis (Figure 8). Although calcium aluminium silicate and microcline were insufficient to place the strength at 1000 °C in the acceptable standardisation zone, their effects were added to the potassium iron silicate, raising the flexural strength for ceramic applications to a favourable condition at 1100 °C. As for the resistance at 1150 °C, where the beginning of the sintering of quartz was recorded, although it helped reduce porosity with its dense phase, in excess, it produced a slight loss in resistance, which was noticeable in our results.

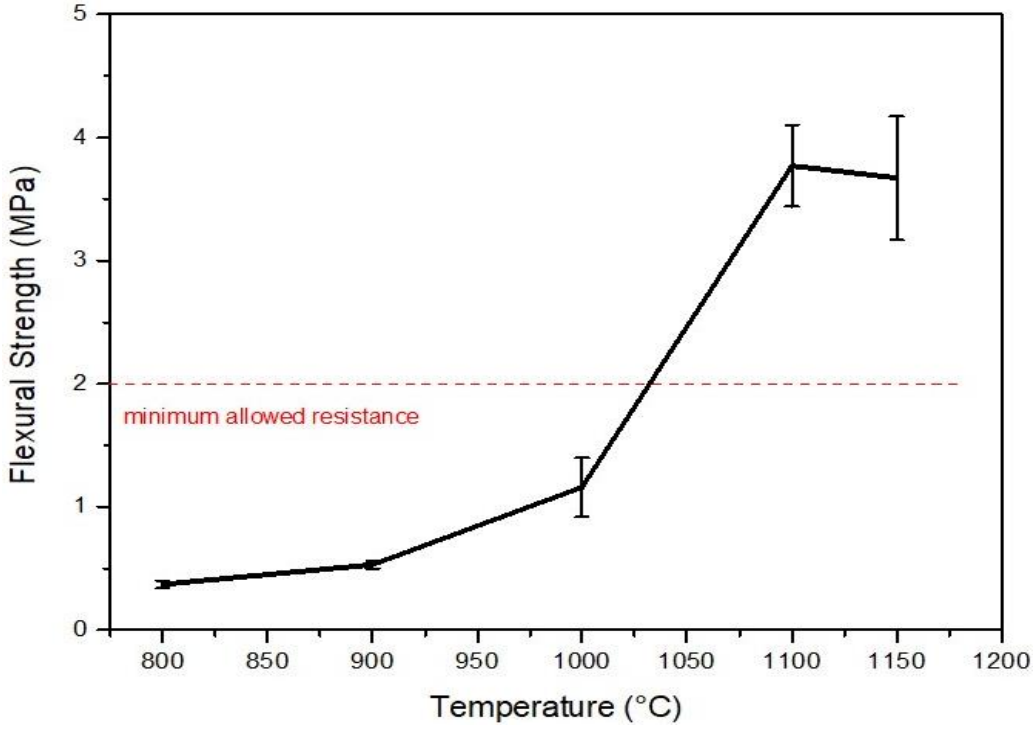


Figure 10. Results of the flexural strength test.

The result of the total linear shrinkage test was used to estimate the dimensioning of the parts produced in the face of the temperatures, shown in Figure 11. It is known that, generally, shrinkage is the result of the elimination of water and decomposition of organic matter, as the granulometric composition of the material strongly influences it, since the smaller the granulometry, the greater the results measured for the retraction in the burned bodies [25].

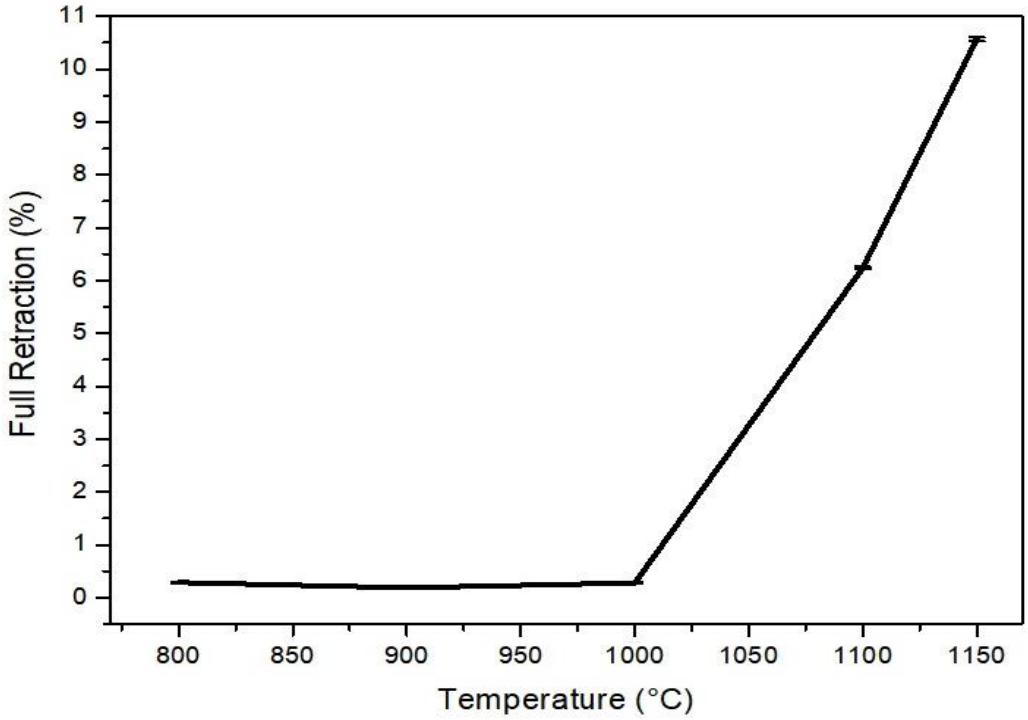


Figure 11. Result of the total linear shrinkage test.

Although the microgranulometry ensured that more than 60% of the material was composed of fine particles smaller than 2 μm (Table 3 and Figure 3), it was observed that up to 1000 °C, the manifested shrinkage was minimal, around 0.25%. However, there was an increase to 6.24% at 1100 °C, and 10.57% at 1150 °C. These results resonated perfectly with the porosity decay results (Figure 9). Therefore, we can say that the reduction in porosity with the increase in temperature promoted a decrease in void spaces, thus, having a positive impact on the reduction in water absorption and enlargement of the specific mass, allowing a desirable increase in the mechanical resistance of the tested bodies, maintaining the shrinkage suffered by the bodies within acceptable limits.

As the most relevant results were obtained with the samples sintered at 1000 °C, 1100 °C, and 1150 °C, the images of the scanning micrograph of the fracture surfaces of the samples are presented for the temperatures mentioned above (Figure 12). Figure 12a shows a significant amount of pores, the uniformity of morisca grains and quartz grains, and a low level of sintering of clay minerals. However, it is evident in Figure 12b that there was an increase in the level of sintering of the clay minerals, as the porosity reduction was noticeable and significant, as fluxes filled the spaces, improving the accommodation of the particles, improving the densification in the pieces and, therefore, contributing to the increase in mechanical strength. In Figure 12c, the porosity reduction is noticeable, as the level of filling of the spaces between the particles intensified, with a significant restriction on the visualisation of the grains, denoting that the dense phase of quartz was incorporated into the fluxes, making the microstructure of the pieces more compact.

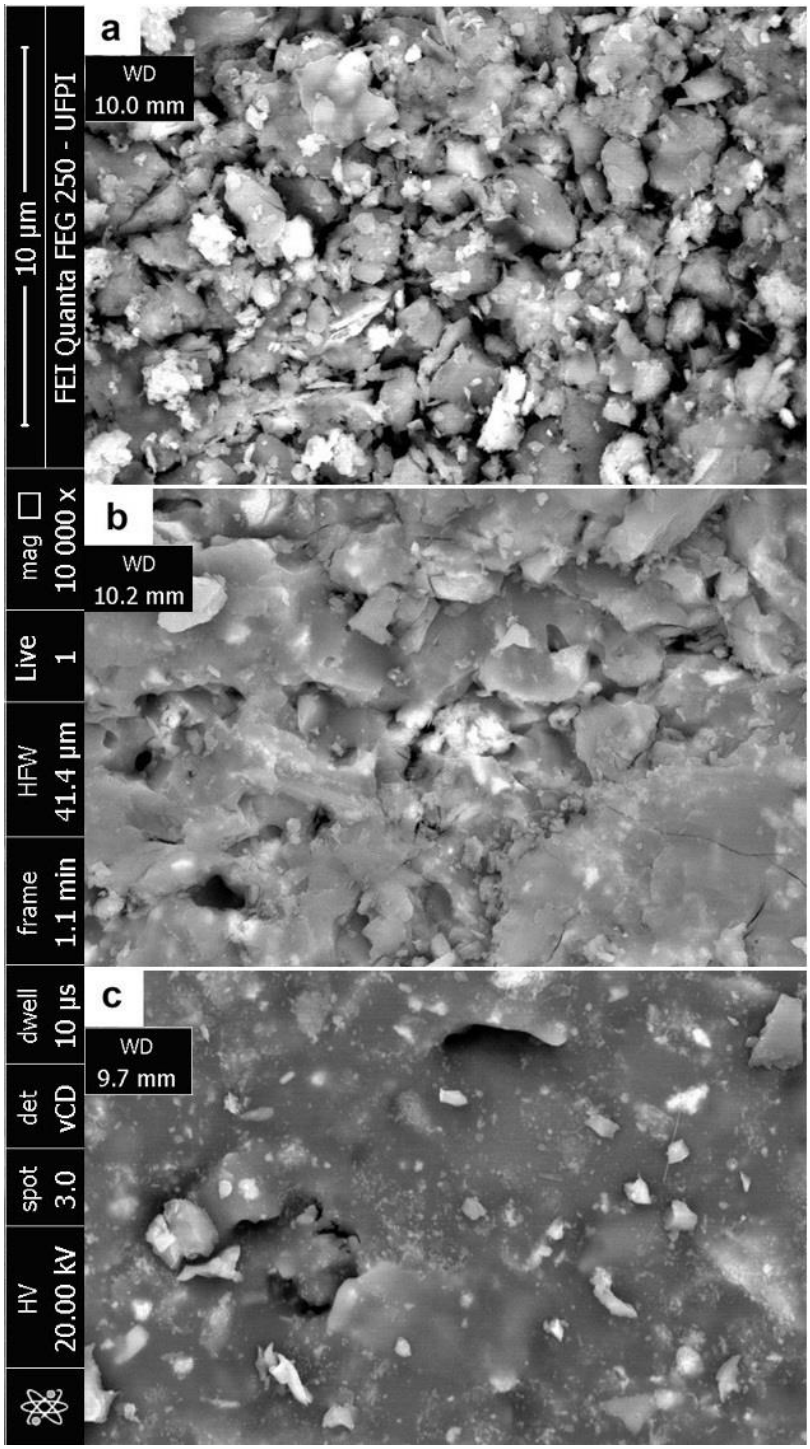


Figure 12. Scanning microscopy at 10,000× magnification: (**a**) sintering image at 1000 °C; (**b**) sintering image at 1100 °C; (**c**) sintering image at 1150 °C.

4. Conclusions

The work described the characteristics of the morisca rock powder to ascertain its technical viability as a substitute material for clays for applications in the red ceramic industry. As a result of this investigation, we confirmed that this material is mainly comprised of silicon oxide, presenting plasticity, which allows the formation of ceramic pieces by pressing or extrusion, as well as having traditional melting clay minerals in its composition, capable of providing the mechanical resistance necessary for ceramic products. We verified with burning tests that using morisca powder requires a temperature of around

1100 °C for applications in masonry, as well as caution with the burning rate, as the material has a considerable concentration of quartz.

Conjecturing the economic viability inherent to ceramic materials, although it was not the focus of this work, we can recall the most common parameters that affect the cost of ceramic production, such as transport of the raw material, the preparation process of the materials involved, the type of energy that will be used for burning (electricity, coal or wood), and oven technology, among others. Murmu [40] clarified that for each type of kiln, there is a different energy consumption, and Zang [41] informed that to produce a burnt brick, an average of 2.0 kWh of energy is spent (parameters were not mentioned). This information demonstrates that many variables interfere with economic analysis. Nevertheless, for morisca, we can guarantee that it will incur the cost of transport, referring to the 50 km distance to the nearest ceramic pole, and the cost of grinding if demand exceeds the disposal of the settling tanks. However, in Brazil, industries that incorporate environmental liabilities into their operations receive tax incentives from the government; tax reductions are an example of these actions.

Given the above, we conclude that the environmental liability of morisca powder has been technically shown to have the necessary potential for its use as a raw material in the red ceramic industry.

Supplementary Materials: The following supporting information can be downloaded at: https://www.mdpi.com/article/10.3390/min13040459/s1, Figure S1: Quartz peaks changes.

Author Contributions: Conceptualization, A.A.d.C.J.; methodology, A.A.d.C.J.; software, A.A.d.C.J.; validation, A.A.d.C.J. and J.M.E.d.M.; formal analysis, A.A.d.C.J.; investigation, A.A.d.C.J. and K.d.S.L.; resources, A.A.d.C.J.; writing—original draft preparation, A.A.d.C.J.; writing—review and editing, J.M.E.d.M.; visualization, K.d.S.L. and J.M.E.d.M.; supervision, J.M.E.d.M.; project administration, J.M.E.d.M.; funding acquisition, A.A.d.C.J. All authors have read and agreed to the published version of the manuscript.

Funding: This research was funded by Interinstitutional Doctoral Program (Dinter—funding number 45/2018).

Data Availability Statement: No data was used for the research described in the article.

Acknowledgments: CAPES and UFPI, and IFPI for their support through the Dinter program. We would like to thanks Bruna Silva, for this paper translation/revision.

Conflicts of Interest: The authors declare there is no conflict of interest.

References

1. Abirochas. Brazilian Association of the Ornamental Rock Industry. *Balance of Brazilian Exports and Imports of Ornamental Stones in 2019*. Report 01/2020. Available online: https://abirochas.com.br/wp-content/uploads/2022/01/Informe-01_2020-Balanco-2019-1.pdf (accessed on 23 March 2021).
2. Silva, E. Governor Visits Mine in Juazeiro do Piauí. 2004. Available online: http://www.piaui.pi.gov.br/materia.php?id=6462 (accessed on 23 March 2021).
3. Wicander, R.; Monroe, J.S. *Fundamentals of Geology*; Cengage Learning: São Paulo, Brazil, 2014.
4. Chioli Filho, C.; Rodrigues, E.P. *Applications Guide for Cladding Rocks: Bula Project*; ABIROCHAS: São Paulo, Brazil, 2009; 119p.
5. Araújo, A.M.M.; Santos, L.C.M.L.; Barbosa, D.; Sousa, A.A.P.; Silva, J.P., Jr.; Barbosa, F.S. Analysis of Quartzite Mining Activity in the Quilombola Sumidouro Community, Queimada Nova—Piauí. CPMTC. *Geonomos* **2017**, *25*, 50–56.
6. Andreola, F.; Barbieri, L.; Lancellotti, I.; Leonelli, C.; Manfredini, T. Recycling of industrial wastes in ceramic manufacturing: State of art and glass case studies. *Ceram. Int.* **2016**, *42*, 13333–13338. [CrossRef]
7. Silva, M.C.A.; Leão, V.A.; Reis, E.L. Incorporation of quartzite fines in the production of red ceramics. *J. Clean. Prod.* **2021**, *288*, 125098. [CrossRef]
8. Carreiro, M.E.A.; Santo, R.C.; Silva, V.J.; Lira, H.L.; Neves, G.A.; Menezes, R.R.; Santana, L.N.L. Residue of quartzite—alternative raw material for use in structural ceramics. *Ceramica* **2016**, *62*, 170–178. [CrossRef]
9. Suvorova, O.V.; Selivanova, E.A.; Mikhailova, J.A.; Masloboev, V.A.; Makarov, D.V. Ceramic products from mining and metallurgical waste. *Appl. Sci.* **2020**, *10*, 3515. [CrossRef]

10. Suvorova, O.; Kumarova, V.; Nekipelov, D.; Selivanova, E.; Makarov, D.; Masloboev, V. Construction ceramics from ore dressing waste in Murmansk region, Russia. *Constr. Build. Mater.* **2017**, *153*, 783–789. [CrossRef]
11. Siqueira, A.A.; Alexandre, J.; Azevedo, A.R.G.; Botelho, L.C.G.; Paes, A.L.C.; Pinheiro, V.D.; Monteiro, S.N. Evaluation of the incorporation of waste from the paper industry into red ceramics. In Proceedings of the 74th ABM Annual Congress International ABM Week 2019, São Paulo, Brazil, 1–3 October 2019.
12. Cipriano, P.B.; Rezende, R.T.O.; Ferraz, A.D.V. Production of red ceramic using clay from gypsum mining and gypsum residue. *Acta Bras.* **2019**, *3*, 25–29. [CrossRef]
13. Gurgel, J.F.S.; Xavier, S.C.R.; Amaral, I.B.C.; Araújo, A.D.; Reis, A.B. Coprocessing of tailings of the garimpo areinha (Diamantina/MG) for red ceramics production. *Rev. Matéria* **2020**, *25*, e12814.
14. Belmonte, L.J.; Ottosen, L.M.; Kirkelund, G.M.; Jensen, P.E.; Vestbø, A.P. Screening of heavy metal containing waste types for use as raw material in Arctic clay-based bricks. *Environ. Sci. Pollut. Res.* **2018**, *25*, 32831–32843. [CrossRef]
15. Saboya, F.; Xavier, G.C.; Alexandre, J. The use of the powder marble by-product to enhance the properties of brick ceramic. *Constr. Build. Mater.* **2007**, *21*, 1950–1960. [CrossRef]
16. Acchar, W.; Vieira, F.A.; Segadães, A.M. Using ornamental stone cutting rejects as raw materials for red clay ceramic products: Properties and microstructure development. *Mater. Sci. Eng. A* **2006**, *435–436*, 606–610. [CrossRef]
17. Segadães, A.M.; Carvalho, M.A.; Acchar, W. Using marble and granite rejects to enhance the processing of clay products. *Appl. Clay Sci.* **2005**, *30*, 42–52. [CrossRef]
18. Souza, H.N.; Reis, E.L.; Lima, R.M.F.; Cipriano, R.A.S. Using soapstone waste with diesel oil adsorbed as raw material for red ceramic products. *Ceram. Int.* **2016**, *42*, 16205–16211. [CrossRef]
19. Pinheiro, B.C.A.; Holanda, J.N.F. Processing of red ceramics incorporated with encapsulated petroleum waste. *J. Mater. Process Technol.* **2009**, *209*, 5606–5610. [CrossRef]
20. *NBR 6457*; Soil Samples—Preparation for Compaction Tests and Characterisation Tests. Brazilian Association of Standards and Techniques (ABNT): São Paulo, Brazil, 2016.
21. *ABNT NBR 6459*; Soil—Liquid Limit Determination. Brazilian Association of Standards and Techniques (ABNT): São Paulo, Brazil, 2017.
22. *NBR 7180*; Soil—Plasticity Limit Determination. Brazilian Association of Standards and Techniques (ABNT): São Paulo, Brazil, 2016.
23. *NBR 15270-3*; Ceramic Components Part 3: Structural and Non-Structural Ceramic Blocks—Test Methods. Brazilian Association of Standards and Techniques (ABNT): São Paulo, Brazil, 2017.
24. *NBR ISO 10545-3*; Ceramic Tiles Part 3: Determination of Water Absorption, Apparent Porosity, Apparent Relative Density and Bulk Density. Brazilian Association of Standards and Techniques (ABNT): São Paulo, Brazil, 2020.
25. Netto, R.C.B. *Ceramic Tests*; SENAI-SP Editora: São Paulo, Brazil, 2019; 448p.
26. Zanelli, C.; Marrocchino, E.; Guarini, G.; Toffano, A.; Vaccaro, C.; Dondi, M. Recycling Construction and Demolition Residues in Clay Bricks. *Appl. Sci.* **2021**, *11*, 8918. [CrossRef]
27. Santos, G.R. Characterization of Clays in the Municipalities of Sidrolândia and Rio Verde in Mato Grosso/MS. Master's Thesis, Federal University of Mato Grosso do Sul, Campo Grande, Brazil, 2007.
28. Grun, E. Characterisation of Clays from Canelinha/SC and Study of Ceramic Mass Formulations. Master's Thesis, State University of Santa Catarina, Joinville, Brazil, 2007.
29. Setz, L.F.G.; Silva, A.C. *Ceramic Processing without Mystery*; Blucher Ltd.: São Paulo, Brazil, 2019; p. 255.
30. Tognotti, R.; Gracher, H. Firing Defects Caused by Quartz in Monoporozas. *Cerâmica Ind.* **2001**, *6*, 40–45.
31. Barnes, G. *Soil Mechanics: Principles and Practice*, 4th ed.; Palgrave Macmillan: London, UK, 2016.
32. Almeida, K.S.; Soares, R.A.L.; Matos, J.M.E. Characterization of clay deposit in the central region of piauí for use in the ceramic industry. *Rev. Matéria* **2020**, *25*, 1–13. [CrossRef]
33. Caputo, H.P. *Soil Mechanics and It's Fundamental Applications*, 6th ed.; LTC: Rio de Janeiro, Brazil, 1996.
34. Hasan, M.; Sayed, A.; Hossain, M.A.; Hossain, M.; Sohel, M.H. Determination of Consistency Limits of Different Agricultural Soils. *Intern. Inv. J. Agric. Soil Scie.* **2017**, *5*, 1–7.
35. Vigneron, T.Q.G.; Vieira, C.M.F.; Delaqua, G.C.G.; Vernilli, F., Jr.; Neto, Â.C. Incorporation of waste in red mold flux ceramic. *J. Mater. Res. Technol.* **2019**, *8*, 5707–5715. [CrossRef]
36. Sesma, N.M. Study of the Properties of a Red Ceramic Sintered at Different Temperatures. Master's Thesis, School of Engineering of Lorena-University of São Paulo, São Paulo, Brazil, 2014.
37. *NBR 15270-1*; Ceramic Components—Part 1: Ceramic Blocks for Sealing Masonry—Terminology and Requirements. Brazilian Association of Standards and Techniques (ABNT): São Paulo, Brazil, 2016.
38. *NBR 15310*; Ceramic Components—Tiles—Terminology, Requirements and Test Methods. Brazilian Association of Standards and Techniques (ABNT): São Paulo, Brazil, 2005.
39. Dantas, A.P.A.; Acchar, W.; Leite, J.Y.P.L.; Araújo, F.S.D. Utilisation of Residue of Ornamental Rocks in the Porcelained Stoneware. *Holos* **2010**, *26*, 92–108. [CrossRef]

40. Murmu, A.L.; Patel, A. Towards sustainable bricks production: An overview. *Constr. Build. Mater.* **2018**, *165*, 112–125. [CrossRef]
41. Zhang, L. Production of bricks from waste materials—A review. *Constr. Build. Mater.* **2013**, *47*, 643–655. [CrossRef]

Disclaimer/Publisher's Note: The statements, opinions and data contained in all publications are solely those of the individual author(s) and contributor(s) and not of MDPI and/or the editor(s). MDPI and/or the editor(s) disclaim responsibility for any injury to people or property resulting from any ideas, methods, instructions or products referred to in the content.